Int J Earth Sci (Geol Rundsch) (2004) 93: 974–989
DOI 10.1007/s00531-004-0432-5

ORIGINAL PAPER

Serhat Köksal · Rolf L. Romer · M. Cemal Göncüoglu
Rolf L. Romer · Fatma Toksoy-Köksal

Timing of post-collisional H-type to A-type granitic magmatism: U–Pb titanite ages from the Alpine central Anatolian granitoids (Turkey)

Received: 20 December 2002 / Accepted: 18 July 2004 / Published online: 29 September 2004

Abstract The last stages of the continental collision during the closure of the Neotethyan ocean in central Anatolia are characterized by post-collisional H- and A-type granitoids intruding both the metamorphic country rocks and allochthonous ophiolitic rocks of the central Anatolian crystalline complex. Available Rb–Sr and K–Ar whole-rock and mineral age data on the H- and A-type granitoids in central Anatolia are inconsistent. To better constrain the geological relevance and the timing of the change in the chemical character of magmatism in the wake of the Alpine orogeny in Anatolia, we re-evaluated the geochemical characteristics and dated titanite from representative H- (Baranadag quartz-monzonite: BR) and A-type (Çamsari quartz-syenite: CS) granitoids by the U–Pb method. BR is a high-K calc-alkaline intrusion with mafic microgranular enclaves and shows enrichment of LILE relative to HFSE. The alkaline CS displays higher SiO_2, $Na_2O + K_2O$, Fe/Mg, Rb, Th and HFSE with corresponding depletion in CaO, MgO, $Fe_2O_3{}^{tot}$, P_2O_5, Ba, Sr, and Ti. Chondrite-normalized REE patterns of the BR and CS samples have LREE-enriched and flat HREE patterns, whereas CS differs from BR by higher LREE enrichment and lower MREE and HREE contents. Mineralogical and geochemical characteristics suggest that BR and CS were not products of the same magma source. BR was derived from a subduction-modified depleted hybrid-source and CS had an enriched mantle source with significant crustal contribution. The U–Pb titanite ages of the H-type central Anatolian granitoids (BR) and the A-type granitoids (CS) are 74.0 ± 2.8 and 74.1 ± 0.7 Ma, respectively. The coeval evolution of post-collisional/calc-alkaline H- to A-type magmatism was possibly associated with source heterogeneity and variable involvement of continental materials during the evolution of these granitoids. These new age data constrain the timing of the onset of a post-collision extensional period following the Alpine thickening within the passive margin of the Tauride–Anatolide platform, which occurred before the opening of the latest Cretaceous central Anatolian basins.

Keywords U–Pb titanite age · H-type · A-type · Granitoid · Central Anatolia

S. Köksal · M. C. Göncüoglu · F. Toksoy-Köksal (✉)
Department of Geological Engineering,
Middle East Technical University,
06531 Ankara, Turkey
E-mail: ftkoksal@metu.edu.tr

R. L. Romer
GeoForschungsZentrum Potsdam, Telegrafenberg,
14473 Potsdam, Germany

Present address: S. Köksal
Central Laboratory, Middle East Technical University,
06931 Ankara, Turkey

Introduction

The understanding of the evolution of post-collisional orogenic systems critically bases on the timing and petrogenesis of the granitoid magmatism postdating the peak of thrusting, regional metamorphism, and deformation (e.g., Pearce et al. 1984; Harris et al. 1986; Förster et al. 1997). Post-collisional granitoids are generally described as calc-alkaline I-type or hybrid late-orogenic (H_{LO} after Barbarin 1990), although A-type granitoids are also known from post-collisional or post-orogenic settings (e.g., Sylvester 1989; Jung et al. 1998; Bonin et al. 1998; Wu et al. 2002). The source of A-type magmas in orogenic belts, however, has remained enigmatic. Collins et al. (1982) suggested that A-type granitoids are products of partial melting of a felsic-granulitic source, which was the residue after generation of I-type granitoids. Similarly, Whalen et al. (1987) suggested that A-type magmas may form by the remelting of F- and/or Cl-enriched dry, granulitic residue remaining in the lower crust after extraction of an orogenic granite. In contrast, Creaser et al. (1991) considered that partial melting of undepleted tonalitic to granodioritic rocks results in A-type granitoids. Other

authors suggested mantle-derived melts as possible source for A-type granitoids. For instance, Eby (1990, 1992) and Turner et al. (1992) invoked alkali basaltic magma that experienced extreme fractional crystallization as a source for A-type granitoids in post-orogenic settings. Whalen et al. (1996) indicated that A-type melts also may be obtained from the remelting of hybridized lithospheric mantle after collision-related delamination or slab break-off. The combination of partial melting of mantle-derived tonalitic sources, interaction of these melts with crustal rocks during the ascent of magma, and crystal fractionation may be efficient in the genesis of the A-type granitoids (Jung et al. 1998). These studies indicate that A-type granitoids may occur in many different settings and extracted from a wide range of different sources (Wu et al. 2002).

In central Anatolia, voluminous H-type (hybrid) with small A-type granitoids occur. The H-type granitoids are commonly thought to have evolved in a post-collisional tectonic setting (Göncüoglu et al. 1991, 1992, 1993; Göncüoglu and Türeli 1993, 1994; Erler and Göncüoglu 1996; Ilbeyli and Pearce 1997; Boztug 1998, 2000; Aydin et al. 1998; Düzgören-Aydin et al. 2001; Kuscu et al. 2002). The A-type intrusive and extrusive rocks are less voluminous and typically intrude H-type granitoids representative for late stage Alpine magmatism in central Anatolia (Göncüoglu et al. 1997; Köksal et al. 2001). Even though several petrological studies on granitoids were carried out, the origin and genetic relation among the granitoids is still under debate. Apart from uncertainties concerning the petrology of the granitoids, there is no reliable geochronological database since published data include mainly Rb–Sr and K–Ar whole-rock and mineral ages that scatter widely. In part, the data are conflicting and thereby form the base for the controversy on the geological evolution of the region.

This study aims to constrain the evolution of H- and A-type granitoids in central Anatolia in terms of time and petrology. Towards this purpose, we present U–Pb age data for the Baranadag quartz-monzonite (BR) representing the H-type late stage post-collision and the Çamsari quartz-syenite (CS) characterizing an early A-type intrusion. Moreover, we assess the validity of published age data used to constrain contrasting geodynamic models for the evolution of Alpine domain in central Anatolia.

Geological framework

Anatolia is located within the east-west trending segment of the Alpine-Himalayan orogenic belt that marks the boundary between Gondwana to the south and Laurasia to the north. All along its Phanerozoic geological history, Anatolia was the site of a complex mosaic of different continental and oceanic assemblages related to the opening and closure of different branches of the Tethys. The present geology of Turkey is characterized by features related to the closure of the Mesozoic Neotethys ocean during the Alpine orogeny (Fig. 1a). It is commonly accepted that one of the northern branches of the Neotethys, the Izmir-Ankara-Erzincan Ocean (IAEO), separated the Gondwanan Tauride–Anatolide platform from the Sakarya microcontinent during Mesozoic times. The IAEO was closed by two northward-directed subduction zones (Göncüoglu and Türeli 1993). The northern branch generated the Late Mesozoic-Tertiary Pontide magmatic arc (Sengör and Yilmaz 1981). The southern, intra-oceanic branch gave way to the formation of an island arc and supra-subduction zone ophiolites within the IAEO during Middle Cretaceous (Göncüoglu and Türeli 1993; Yaliniz et al. 1996). Their collision with the passive margin of the Tauride–Anatolide platform, i.e., the present central Anatolian crystalline complex (CACC), during the Late Cretaceous resulted in the emplacement of ophiolitic nappes onto the CACC and crustal thickening (Göncüoglu et al. 1991). Ilbeyli et al. (2004) suggested that delamination of the metasomatized lithospheric mantle or removal of a subducted slab represent possible mechanisms to generate post-collision granitoids. Göncüoglu et al. (1991, 1992, 1993, 1997) interpreted the transition from collision to post-collisional extension, which gave way to the evolution of granitoids, to have occurred in the Late Cretaceous. In contrast, Sengör and Yilmaz (1981), Görür et al. (1984, 1998), Whitney and Dilek (1997), and Kadioglu et al. (2003) suggested that the CACC was separated from the main body of the Tauride–Anatolide platform since Jurassic by an intervening ''Inner Tauride Ocean''. This ocean was closed by northward subduction beneath the CACC during Early Paleocene-Eocene, generating Andean-type calc-alkaline arc magmatism. Both models are essentially based on tectonic considerations, but lack adequate geochronological constraints.

The CACC contains slices of metamorphic, ophiolitic, granitic, and syenitic rocks (Fig. 1b). The metamorphic rocks include a Precambrian basement of ortho- and paragneisses with rare amphibolite and metacarbonate. The lower part of the cover of the Precambrian basement consists of metaclastic rocks and marbles similar to the Paleozoic successions of the Tauride Platform. The upper part of the cover includes a thick package of marbles, which are equivalents of the Mesozoic carbonates in the Taurides (Göncüoglu 1986). This package is overlain by an ophiolite-bearing sedimentary mélange. These HT/LP metamorphic rocks are tectonically overlain by a nappe that includes MORB, island arc related rocks, and low-grade metamorphic remnants of a supra-subduction-type Neotethyan oceanic lithosphere. Granites and syenites intruded both the metamorphic rocks and the sedimentary mélange. The youngest magmatic rocks include syenites. Their extrusive equivalents are found as blocks and boulders within the oldest non-metamorphic cover units of Upper Maastrichtian to Lower Paleocene age (Köksal et al. 2001). East–west trending fault-controlled

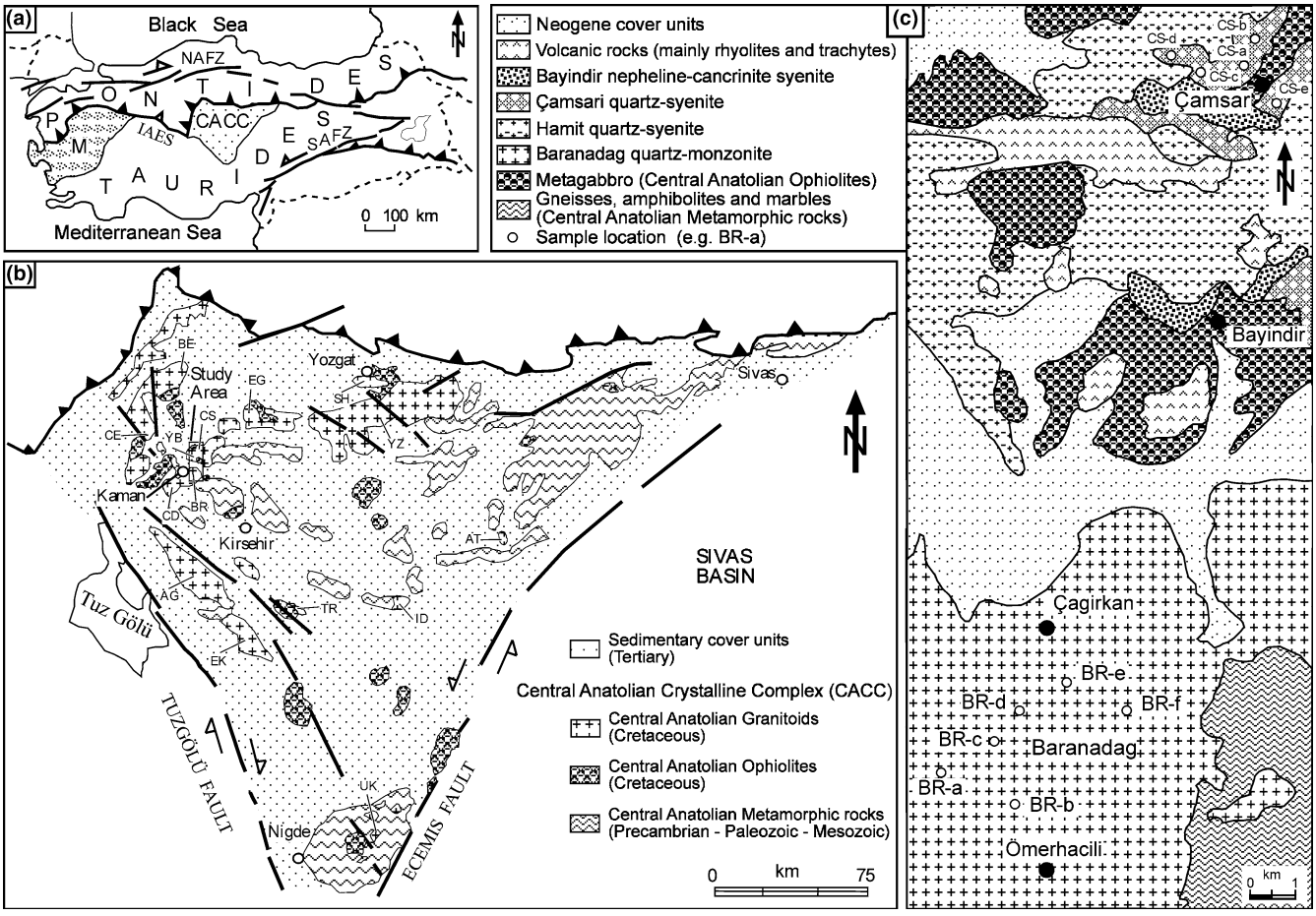

Fig. 1 **a** Locations of main tectonic units and the structure belts in Turkey (modified after Toksoy-Köksal et al. 2001). *M* Menderes Massif, *IAES* Izmir-Ankara-Erzincan Suture Zone, *NAFZ* North Anatolian Fault Zone, *SAFZ* South Anatolian Fault Zone; **b** simplified geological map of the CACC (Modified after Düzgören-Aydin et al. 2001; Toksoy-Köksal et al. 2001). Central Anatolian granitoids: *H-type- BR* Baranadag, *CD* Cefalikdag, *AG* Agaçören, *TR* Terlemez, *EK* Ekecikdag, *CE* Çelebi, *BE* Behrekdag, *YZ* Yozgat, *S-type- UK* Üçkapili, *SH* Sarihacili, *A-type- CS* Çamsari, *EG* Egrialan, *ID* Idisdag, *YB* Bayindir, *AT* Atdere; **c** simplified geological map and sample locations of the Baranadag and Çamsari granitoids (Modified after Göncüoglu et al. 1992; Otlu and Boztug 1998)

basins (e.g., Central Kızılırmak Basin, Dirik et al. 1999) within and around the CACC include, apart from Upper Maastrichtian to Lower Paleocene continental to shallow-marine sediments, also an Early to Middle Eocene succession that starts with transgressive carbonates and terminates with a regressive series. The Eocene succession also includes within-plate type volcanic and volcanoclastic rocks and is unconformably overlain by Lower Miocene evaporites and continental clastic rocks. A distinct compressional event, prior to the deposition of Upper Miocene-Pliocene continental clastic, volcanoclastic, and volcanic rocks, is marked by the overthrusting of basement lithologies onto Lower Miocene sediments (Göncüoglu et al. 1991).

Existing age constraints

Earlier efforts to constrain the timing of magmatism in central Anatolia are listed in Table 1. The first geochronological study on the granitoids gave an age of c. 54 Ma using the total-Pb method (chemical age) on a single zircon grain from the BR (Ayan 1963). Recently, K–Ar mineral ages from Baranadag granitoids was determined by Ilbeyli et al. (2004) as 76.4 ± 1.3 Ma. Ilbeyli et al. (2004) also determined the age of Cefalikdag granitoids, from the Kaman region, as 66.6 ± 1.1 Ma by K–Ar method. Ataman (1972) presented an Rb–Sr 3-point whole-rock (WR) isochron age of 73.5 ± 1.0 Ma [age recalculated using the decay constants recommended by IUGS (Steiger and Jäger 1977)] for the Cefalikdag granitoid. This age is in agreement with K–Ar mineral ages ranging from 69 to 74 Ma (Erkan and Ataman 1981), obtained from metamorphic rocks to constrain the intrusion and cooling age of the Cefalikdag granitic rocks. Furthermore, some of the alkaline intrusions from the Kaman region gave Rb–Sr WR isochron ages between 70.5 and 85.1 Ma (Table 1).

Age data to the south and southeast of the Kaman region span a wider range. For instance, the Agaçören granitoid yields an Rb–Sr 3-point WR isochron age of 110 ± 14 Ma that has been interpreted as intrusion age

Table 1 Previous geochronological data from the central Anatolian granitoids

Name of Intrusion	Method	Age (Ma)	Granitoid type	Authors
Bayindir feldspathoidal syenite (Kaman)	Rb–Sr (WR)	70.7 ± 1.1	A-type	Gündogdu et al. (1988)
Bayindir quartz syenite (Kaman)	Rb–Sr (WR)	85.1 ± 3.6	A-type	Kuruç (1990)
Bayindir sodalite syenite (Kaman)	Rb–Sr (WR)	84.4 ± 0.9	A-type	Kuruç (1990)
Bayindir miaskite (Kaman)	Rb–Sr (WR)	71.8 ± 0.1	A-type	Kuruç (1990)
Bayindir foyaites and volcanic rocks (Kaman)	Rb–Sr (WR)	70.5 ± 3.4	A-type	Kuruç (1990)
Baranadag quartz monzonite (Kaman)	Total Pb method (zircon)	54	H-type	Ayan (1963)
Baranadag monzonite (Kaman)	K–Ar (mineral)	76.4 ± 1.3	H-type	Ilbeyli et al. (2004)
Cefalikdag granitoid (Kaman)	Rb–Sr (WR)	73.5 ± 1.0[a]	H-type	Ataman (1972)
Cefalikdag quartz-monzonite (Kaman)	K–Ar (mineral)	66.6 ± 1.1	H-type	Ilbeyli et al. (2004)
Agaçören granitoid	Rb–Sr (WR)	110 ± 14	H-type	Güleç (1994)
Agaçören granitoid	Ar–Ar (mineral)	77.6 ± 0.3	H-type	Kadioglu et al. (2003)
Terlemez quartz-monzonite	K–Ar (mineral)	81–67	H-type	Yaliniz et al. (1997)
Behrekdag composite pluton	K–Ar (mineral)	81.2–68.8	H-type	Tatar et al. (2003)
Behrekdag granite	K–Ar (mineral)	79.5 ± 1.7	H-type	Ilbeyli et al. (2004)
Behrekdag composite pluton	K–Ar (mineral)	71.5–69.1	S-type	Tatar et al. (2003)
Üçkapili granitoid	Rb–Sr (WR)	95 ± 11	S-type	Göncüoglu (1986)
Üçkapili granitoid	Rb–Sr (mineral)	77.8 ± 1.2	S-type	Göncüoglu (1986)
Üçkapili granitoid	K–Ar (mineral)	78–75	S-type	Göncüoglu (1986)
Üçkapili granitoid	U–Pb (monazite)	20–13.7	S-type	Whitney and Dilek (1997)
Üçkapili granitoid	U–Pb SHRIMP (zircon)	92–85	S-type	Whitney et al. (2003)
Üçkapili granitoid	^{40} Ar–^{39} Ar plateau age (mineral)	79.5 ± 1.2	S-type	Whitney et al. (2003)

[a]Recalculated using the decay constant recommended by Steiger and Jäger (1977)

(Güleç 1994). Ar–Ar biotite data from the same intrusion, however, yield an age of 77.6 ± 0.3 Ma (Kadioglu et al. 2003). K–Ar age determinations from Terlemez quartz-monzonite ranging from 81.5 ± 1.9 to 67.1 ± 1.3 Ma have been interpreted to reflect intrusion and cooling (Yaliniz et al. 1999).

Rb–Sr and K–Ar age determinations from the syn-collisional Üçkapili Granitoid in the southern part of the CACC (Göncüoglu 1986) span a similar wide range (Rb–Sr WR isochron 95 ± 11 Ma and Rb–Sr mineral isochron 77.8 ± 1.2 Ma). The distinctly older Rb–Sr WR age for the Üçkapili Granitoid, however, bases on four samples from three different exposures, several kilometers apart. This age may have been derived from a rotated mixing line rather than from an isochron (cf. Wendt 1993; Romer 1994). Unpublished U–Pb monazite data were interpreted to yield ages between 20 and 13.7 Ma (Whitney and Dilek 1997). U–Pb SHRIMP studies have shown that zircon cores in Üçkapili Granitoid record Proterozoic through Mesozoic ages, whereas rims consistently yield Late Cretaceous (92–85 Ma) ages, which is in accordance with Ar–Ar mineral age data yielding 79.5 ± 1.2 Ma (Whitney et al. 2003). Age data to the northwest of the Kaman region are only available for Behrekdag composite pluton, which yields K–Ar mineral ages of 69.1 ± 1.4 to 71.5 ± 1.5 Ma for S-type granitoids, and 68.8 ± 1.4 to 81.2 ± 3.4 Ma for H-type granitoids (Tatar et al. 2003). Besides, Ilbeyli et al. (2004) presented K–Ar mineral age of 79.5 ± 1.7 Ma for the Behrekdag granitoid.

The major problem with the existing age database (Table 1) is that there occur (a) cases where the isotopic ages indicate a sequence of emplacement that is not compatible with field observations and (b) dating gave an unreasonable broad age range of some 20–30 Ma for some intrusions. The problem originates only partially from regionally sampled WR isochrons. The age of the magmatism is independently bracketed by the biostratigraphic age of sediments intruded by the granitoids and the first appearance of granitoid pebbles in sediments. The Terlemez quartz-monzonite that has a clear intrusive contact with the Middle Turonian–Lower Santonian pelagic rocks (Yaliniz et al. 1997, 1999), i.e., c. 92–86 Ma according to the numerical time scale of Menning and Deutsche Stratigraphische Kommission (2002). The basal conglomerates of the latest Maastrichtian sediments disconformably covering the CACC are dominated by well-rounded pebbles of granites, syenites and monzonites of the underlying central Anatolian granitoids. Thus, the age of the intrusions is bracketed between Early Santonian age values and latest Maastrichtian age values (e.g., Köksal et al. 2001), i.e., 86–65.0 Ma according to the numerical time scale of Menning and Deutsche Stratigraphische Kommission (2002).

Petrological characteristics of the granitoids

Field and petrographical features

The BR and the CS are exposed to the north of Kirsehir in the western part of the CACC (Fig. 1b). Samples were collected from the same localities (Fig. 1c) as reported by other authors (e.g., Seymen 1981; Lünel 1985; Bayhan 1987; Erler et al. 1991; Otlu and Boztug 1998; Aydin and Önen 1999). Samples for geochronological and geochemical work were chosen from outcrops free of enclaves and altered surfaces.

Table 2 Electron microprobe analyses, cation proportions, and end member compositions of feldspar and pyroxene from the CS

Feldspar

Analyses#	F-1	F-2	F-3	F-4	F-5	F-6	F-7	F-8	F-10	F-11	F-12	F-13	F-14	F-15	F-16
SiO_2	68.72	68.45	68.96	66.11	66.87	65.96	66.41	64.15	65.41	65.95	65.99	66.65	67.58	65.90	65.97
TiO_2	0.01	0.00	0.01	0.00	0.00	0.00	0.01	0.00	0.00	0.01	0.00	0.00	0.00	0.00	0.00
Al_2O_3	20.24	20.36	19.96	18.31	18.85	18.44	18.57	22.88	22.04	18.49	21.82	21.58	19.25	18.49	18.39
MgO	0.00	0.01	0.02	0.00	0.01	0.00	0.00	0.01	0.01	0.01	0.00	0.00	0.00	0.01	0.00
CaO	0.77	0.91	0.57	0.02	0.07	0.05	0.03	4.30	3.37	0.03	2.93	2.56	0.42	0.06	0.02
MnO	0.00	0.03	0.00	0.00	0.00	0.00	0.01	0.00	0.00	0.02	0.02	0.00	0.00	0.01	0.00
FeO	0.08	0.11	0.22	0.19	0.16	0.21	0.09	0.36	0.33	0.21	0.30	0.28	0.13	0.09	0.10
Na_2O	11.21	11.29	10.53	1.92	5.41	2.03	2.73	9.00	9.51	1.77	9.95	10.10	8.24	2.12	1.50
K_2O	0.31	0.20	1.16	13.97	9.77	13.97	12.80	0.55	0.64	14.13	0.32	0.51	5.25	13.66	14.41
Total	101.33	101.37	101.43	100.52	101.14	100.65	100.66	101.25	101.31	100.60	101.33	101.67	100.88	100.33	100.3
Si	11.88	11.83	11.93	12.05	11.97	12.02	12.03	11.23	11.42	12.02	11.49	11.56	11.94	12.02	12.05
Ti	0.00	0.00	0.00	0.00	0.00	0.00	0.00	0.00	0.00	0.00	0.00	0.00	0.00	0.00	0.00
Al	4.12	4.15	4.07	3.93	3.98	3.96	3.97	4.72	4.53	3.97	4.48	4.41	4.01	3.97	3.96
Mg	0.00	0.00	0.00	0.00	0.00	0.00	0.00	0.00	0.00	0.00	0.00	0.00	0.00	0.00	0.00
Ca	0.14	0.17	0.11	0.00	0.01	0.01	0.01	0.81	0.63	0.01	0.55	0.48	0.08	0.01	0.00
Mn	0.00	0.00	0.00	0.00	0.00	0.00	0.00	0.00	0.00	0.00	0.00	0.00	0.00	0.00	0.00
Fe	0.01	0.02	0.03	0.03	0.02	0.03	0.01	0.05	0.05	0.03	0.04	0.04	0.02	0.01	0.01
Na	3.75	3.79	3.53	0.68	1.88	0.72	0.96	3.05	3.22	0.62	3.36	3.40	2.82	0.75	0.53
K	0.07	0.04	0.26	3.25	2.23	3.25	2.96	0.12	0.14	3.29	0.07	0.11	1.18	3.18	3.36
Cation	19.97	20.01	19.93	19.95	20.10	19.98	19.94	19.99	19.99	19.95	19.99	19.99	20.06	19.96	19.92
Or	1.70	1.12	6.57	82.61	54.14	81.72	75.38	3.09	3.56	83.92	1.79	2.80	28.96	80.63	86.26
Ab	94.70	94.66	90.71	17.27	45.53	18.04	24.45	76.66	80.64	15.93	84.46	85.26	69.08	19.06	13.62
An	3.60	4.22	2.73	0.12	0.34	0.24	0.17	20.25	15.80	0.14	13.76	11.94	1.96	0.31	0.12

Analyses were performed by a CAMECA SX-100 type microprobe at Geoforschungs Zentrum Potsdam, Germany
Structural formulae of feldspar calculation is based on 32 oxygens. Pyroxene classification is according to Morimoto (1988) and estima

Baranadag quartz-monzonite was chosen as a representative H-type granitoid in the CACC regarding its geological and petrological similarities with the other central Anatolian hybrid granitoids (Aydin and Önen 1999). BR cuts the metamorphic rocks and overlying ophiolitic units of the CACC (Otlu and Boztug 1998).

Baranadag quartz-monzonite is abundantly composed of K-feldspar (orthoclase, microcline, 32–58 vol%), plagioclase (An_{28-36}, 26–45 vol%), and quartz (4–14 vol%) (Aydin and Önen 1999). There are variable amounts of mafic minerals with modal compositions of 2–17 vol% calcic amphibole (hornblende, tschermakitic hornblende), 1–7 vol% clinopyroxene (diopside with $Wo_{50}En_{34}Fs_{16}$), and 0.5–6 vol% biotite, which is partly altered to chlorite (Aydin and Önen 1999). Titanite, zircon, apatite, and opaque minerals are common accessory minerals. The medium to coarse-grained BR is characterized by a porphyritic texture with pinkish K-feldspar megacrysts. BR includes abundant mafic microgranular enclaves that are elliptical to spherical with sharp contact to their host. The enclaves are finer grained than their host rock and suggest a magma mingling process (Didier and Barbarin 1991). K-feldspar megacrysts, mafic microgranular enclaves, and abundance of mafic minerals (with hornblende > biotite) are common features in H-type central Anatolian granitoids, are commonly interpreted to result from magma mingling/mixing processes (Güleç and Kadioglu 1998; Kadioglu and Güleç 1999), and resemble the H-type granitoid series of Barbarin (1990).

Çamsari quartz-syenite is representative for the silica-saturated A-type plutonic rocks within the CACC (Otlu and Boztug 1998; Boztug 1998, 2000) (Fig. 1c). It is composed of feldspar (78–82 vol%), quartz (12–13 vol%), cpx (5–6 vol%), and small amounts of titanite, fluorite, zircon, titanite, and opaque minerals. CS feldspar is subsolvus with two discrete phases: alkali feldspar is dominant with a wide range in composition from low to high-K content and plagioclase with compositions ranging An_{21} to An_0. Representative microprobe analyses are shown in Table 2. Hedenbergite ($Wo_{47}En_{23}Fs_{31}$), which is pseudomorph after amphibole, is the only mafic mineral. Medium to fine-grained CS rocks show no microgranular mafic or wall rock

							Pyroxene								
F-17	F-18	F-19	F-20	F-21	F-22	F-23	Analyses#	P-1	P-2	P-3	P-4	P-5	P-6	P-7	P-8	P-9
65.28	64.33	64.37	64.14	66.53	66.51	67.81	SiO_2	49.41	49.96	50.39	50.25	50.20	50.10	48.89	50.49	50.03
0.00	0.02	0.03	0.00	0.00	0.01	0.00	TiO_2	0.24	0.20	0.21	0.22	0.21	0.27	0.19	0.20	0.25
18.18	22.66	22.77	22.97	18.92	18.88	19.09	Al_2O_3	2.06	1.82	1.84	1.86	1.82	2.02	2.88	1.93	1.87
0.00	0.01	0.00	0.02	0.00	0.01	0.02	FeO^{tot}	18.40	16.9	16.8	16.6	16.4	17.1	16.7	16.2	16.8
0.01	4.21	4.17	4.33	0.27	0.36	0.32	MnO	1.52	1.45	1.34	1.37	1.49	1.32	1.22	1.44	1.44
0.00	0.03	0.02	0.00	0.06	0.04	0.02	MgO	6.48	7.21	7.64	7.78	7.78	7.49	8.25	7.72	7.45
0.14	0.38	0.33	0.27	0.18	0.19	0.21	CaO	21.90	22.20	22.40	22.40	22.40	22.40	18.00	22.30	22.20
1.12	9.23	9.26	8.97	3.93	4.10	6.89	Na_2O	1.10	1.10	1.04	1.06	1.03	1.09	0.86	1.07	1.05
14.95	0.57	0.47	0.65	11.07	10.61	6.67	K_2O	0.00	0.00	0.00	0.01	0.00	0.00	0.10	0.00	0.01
99.68	101.43	101.42	101.36	100.96	100.69	101.02	Total	101.11	100.84	101.66	101.55	101.33	101.75	97.09	101.35	101.10
12.04	11.25	11.25	11.22	11.97	11.97	12.00	TSi	1.90	1.92	1.91	1.91	1.91	1.91	1.90	1.94	1.92
0.00	0.00	0.00	0.00	0.00	0.00	0.00	TAl	0.09	0.08	0.08	0.08	0.08	0.08	0.09	0.06	0.08
3.95	4.67	4.69	4.74	4.01	4.01	3.98	TFe^{3+}	0.01	0.00	0.01	0.01	0.01	0.01	0.01	0.00	0.00
0.00	0.00	0.00	0.01	0.00	0.00	0.00	M_1Al	0.00	0.00	0.00	0.00	0.00	0.00	0.00	0.07	0.01
0.00	0.79	0.78	0.81	0.05	0.07	0.06	M_1Fe^{3+}	0.17	0.16	0.15	0.16	0.16	0.15	0.16	0.04	0.14
0.00	0.00	0.00	0.00	0.01	0.01	0.00	M_1Ti	0.01	0.01	0.01	0.01	0.01	0.01	0.01	0.01	0.01
0.02	0.06	0.05	0.04	0.03	0.03	0.03	M_1Mg	0.37	0.41	0.43	0.44	0.44	0.44	0.42	0.43	0.44
0.40	3.13	3.14	3.04	1.37	1.43	2.36	M_1Fe^{2+}	0.40	0.39	0.38	0.36	0.36	0.36	0.37	0.43	0.37
3.52	0.13	0.10	0.15	2.54	2.44	1.51	M_1Mn	0.05	0.04	0.03	0.03	0.03	0.04	0.03	0.02	0.04
19.94	20.04	20.02	20.00	19.98	19.96	19.95	M_2Mg	0.00	0.00	0.00	0.00	0.00	0.00	0.00	0.06	0.00
89.71	3.15	2.60	3.63	64.09	61.90	38.33	M_2Fe^{2+}	0.02	0.00	0.00	0.00	0.00	0.00	0.00	0.08	0.00
10.23	77.36	78.00	76.08	34.60	36.35	60.13	M_2Mn	0.00	0.01	0.01	0.01	0.01	0.01	0.01	0.02	0.01
0.06	19.48	19.39	20.29	1.30	1.74	1.55	M_2Ca	0.90	0.91	0.91	0.91	0.91	0.91	0.91	0.77	0.91
							M_2Na	0.08	0.08	0.08	0.08	0.08	0.08	0.08	0.07	0.08
							M_2K	0.00	0.00	0.00	0.00	0.00	0.00	0.00	0.00	0.00
							Cation	4.00	4.00	4.00	4.00	4.00	4.00	4.00	4.00	4.00
							Wo%	47.17	47.69	47.40	47.41	47.41	47.44	47.42	41.38	47.66
							En%	19.40	21.51	22.52	22.93	22.93	22.91	22.10	26.39	22.91
							Fs%	33.43	30.81	30.08	29.66	29.66	29.65	30.48	32.24	29.43
							$Fe^{2+}/(Fe^{2+}+Mg)$	0.53	0.48	0.47	0.45	0.45	0.45	0.47	0.51	0.46

tion of ferric iron is from Droop (1987)

enclaves. Although contact relations between the BR and CS rocks are not exposed in the studied area, there occur small-scale quartz-syenite bodies and dikes, showing mineralogical and petrographical similarities to CS that cut Baranadag. In other parts of the CACC, CS-like quartz-syenites are known to cut BR-like quartz-monzonites (Akiman et al. 1993).

Geochemistry

BR and CS are typical CACC granitoids. We characterize the geochemical composition of these granites using data for the 11 samples shown in Table 3 and major and some trace element contents for additional 38 samples from the literature (Otlu and Boztug 1998) and Boztug (1998, 2000). BR and CS are characterized by high contents of total alkali elements (Table 3). CS shows distinctly higher SiO_2 contents than BR. BR exhibits a metaluminous calc-alkaline character with $A/CNK < 1$ and $A/NK > 1$, and agpaitic index $(AI) < 0.87$ (Fig. 2). In contrast, CS is characterized by weakly metaluminous to peraluminous ($A/CNK = 0.92–1.20$, $A/NK > 1$) and calc-alkaline to alkaline composition ($AI = 0.80–0.94$).

The BR and CS samples exhibit distinct geochemical trends in Harker diagrams (Fig. 3). In general, BR displays higher concentrations of TiO_2, $Fe_2O_3^{tot}$, MgO, CaO, P_2O_5, Ba, Sr, and lower abundances of SiO_2, Na_2O, K_2O, Rb, Nb, Th, and Zr than the CS samples. The compositional variation trends against SiO_2 for BR and CS do not form continuous pattern. Instead, the variation trends are offset from each other (e.g., as for $Fe_2O_3^{tot}$, CaO, Fig. 3) or have contrasting slopes (e.g., as for P_2O_5, Ba, and Sr, Fig. 3). Thus, the contrasting nature of the BR and CS rocks does not reflect differently evolved rocks from the same suite, as might be suggested by the contrasting ranges of SiO_2 content, but reflect distinct paths of magma evolution and derivation from separate sources. This contrast between the BR and CS rocks becomes even more obvious in a multi-element plot normalized to continental crust (Fig. 4). The BR rocks display an enrichment in LILE (Rb, Ba, Th, U, K, Sr) and LREE relative to HSFE (Nb, Ta, Zr, Hf, Sm, Y) and

Table 3 Geochemical analyses of the BR and CS granitoids

	Baranadag quartz monzonite						Çamsari quartz syenite				
	BR-a	BR-b	BR-c	BR-d	BR-e	BR-f[a]	CS-a[a]	CS-b	CS-c	CS-d	CS-e
SiO_2	59.5	59.6	59.9	59.3	58.4	59.67	63.7	63.2	62.7	69.6	65.1
Al_2O_3	17.0	17.2	17.4	17.3	17.2	17.3	18.1	18.9	18.1	15.6	18.2
$Fe_2O_3^{tot}$	5.07	5.18	4.80	5.01	5.45	4.98	2.63	2.86	2.51	1.73	1.44
MgO	1.63	1.72	1.57	1.58	1.82	1.54	0.28	0.26	0.23	0.14	0.07
CaO	4.76	5.03	4.87	4.87	5.59	4.87	1.74	2.00	1.42	1.35	0.42
Na_2O	3.50	3.63	3.62	3.47	3.46	3.49	4.77	5.62	4.00	3.99	4.09
K_2O	6.02	5.70	6.00	6.59	5.84	6.35	7.95	6.30	9.62	6.67	9.48
TiO_2	0.53	0.55	0.51	0.52	0.56	0.53	0.35	0.28	0.38	0.21	0.15
P_2O_5	0.23	0.26	0.25	0.29	0.28	0.24	< 0.01	0.01	0.03	< 0.01	< 0.01
MnO	0.10	0.10	0.10	0.11	0.11	0.10	0.06	0.07	0.09	0.02	0.03
LOI	1.2	0.6	0.6	0.6	0.8	0.8	0.6	0.2	0.7	0.5	0.7
Total	99.7	99.7	99.7	99.8	99.7	99.9	100.2	99.7	99.8	99.8	99.7
Ba	1,080	1,050	1,090	1,130	1,290	1,110	261	183	136	199	218
Sc	6	6	6	8	7	6	1	1	1	1	1
Cr	205	212	226	219	192	274	328	178	151	246	164
Co	11	11	9	10	10	11	3	2	2	1	1
Cs	8.9	8.6	13	9.4	9.4	9.3	15	4.9	19	19	16
Ga	21	21	21	19	21	21	22	21	21	18	19
Hf	5.7	6.3	5.8	5.6	6.4	7.6	10	11	9.8	7.5	18
Nb	21	23	22	19	23	24	47	38	69	22	27
Rb	245	232	233	210	205	233	335	219	450	376	467
Sn	4	3	4	3	3	5	3	3	4	3	2
Sr	970	964	952	964	1,070	1,010	309	215	160	250	117
Ta	1.2	1.4	1.4	1.1	1.4	1.3	2.0	1.4	3.6	1.0	1.1
Th	32	35	22	30	29	27	59	96	114	121	33
U	7.4	6.2	8.1	5.2	5.4	6.8	13	13	30	16	12
V	96	95	87	87	103	97	40	33	22	18	15
Zr	251	254	219	216	256	275	518	655	479	248	971
Y	27	28	28	23	29	29	24	23	28	14	13
Mo	6.9	6.4	6.8	6.7	5.9	6.8	11	6.6	5.2	10	7.5
Cu	15	17	16	18	17	19	14	8.5	6.1	10	9.3
Pb	4.1	4.6	7.7	6.3	5.2	6.8	29	24	23	15	17
Zn	36	35	35	40	36	47	31	27	67	22	17
Ni	14	15	15	17	13	28	22	13	8.7	16	15
As	1.4	1.8	6.5	3.0	2.6	2.7	3.9	3.0	11	3.9	4.0
Bi	0.1	0.1	0.3	0.2	0.2	0.2	0.2	0.2	0.7	0.5	0.8
La	62	62	65	60	80	75	148	117	106	90	143
Ce	129	134	134	118	157	151	248	206	213	132	182
Pr	14	15	15	13	16	14	18	18	19	10	12
Nd	54	55	55	49	61	57	59	52	65	29	32
Sm	9.2	9.0	9.3	8.2	10.6	9.5	7.5	6.6	9.3	3.7	3.2
Eu	2.0	2.0	2.0	1.7	2.2	2.0	1.4	1.1	1.3	0.73	0.65
Gd	6.29	6.50	6.73	5.97	7.11	7.26	6.32	3.94	5.73	2.4	1.6
Tb	0.85	0.90	0.89	0.80	0.98	0.94	0.71	0.63	0.84	0.36	0.33
Dy	4.7	4.6	4.7	4.1	5.2	5.0	3.9	3.4	4.4	2.1	1.9
Ho	0.87	0.91	0.86	0.78	0.94	0.79	0.66	0.65	0.82	0.39	0.41
Er	2.2	2.2	2.4	2.0	2.6	2.4	2.2	1.9	2.3	1.3	1.3
Tm	0.31	0.36	0.31	0.29	0.36	0.32	0.29	0.30	0.37	0.19	0.21
Yb	2.2	2.3	2.4	2.1	2.5	2.5	2.4	2.6	2.6	1.6	1.8
Lu	0.34	0.36	0.30	0.28	0.33	0.36	0.37	0.36	0.38	0.27	0.30

Geochemical analyses were performed in ACME Analytical Laboratories Ltd. (Canada). Major elements, Ba, and Sc were measured by ICP-AES

tot total Fe as Fe_2O_3

Major elements in wt%, trace elements in ppm, trace elements excluding Ba and Sc were measured by ICP-MS, and LOI is loss of ignition

[a]Samples used for U–Pb dating

HREE. BR is characterized by small negative anomalies in Ba, Nb, Ta, Ti, Zr and Hf. CS is strongly enriched in LILE and LREE relative to HFSE and shows a strong depletion in Ba, Sr, and Ti and enrichment in Rb, Th, U, Zr, and Hf. Even though CS is depleted in Nb, Ta, it has higher concentration of these elements than BR.

The contrast between the BR and CS rocks is also obvious in chondrite-normalized REE pattern (Fig. 5). The BR and CS samples have steep LREE-enriched and flat HREE patterns (Fig. 5). CS shows a higher LREE enrichment and lower MREE and HREE contents than BR. CS exhibits variable and more pronounced negative Eu anomalies ($(Eu/Eu^*)_N = 0.53–0.88$) and higher $(La/Yb)_N$ ratios (27–54). In contrast, BR has small negative Eu anomalies ($(Eu/Eu^*)_N = 0.74–0.81$) and high $(La/Yb)_N$ ratios (18–21). REE patterns of both BR and

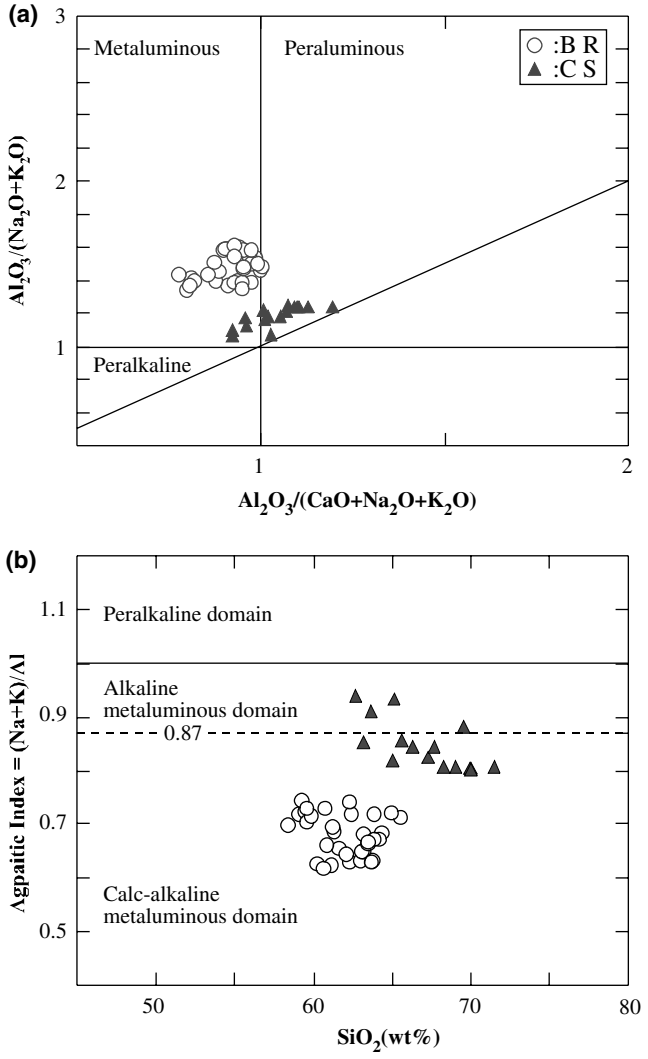

Fig. 2 **a** Plot of Shand index for BR and CS, discrimination fields are from Maniar and Piccoli (1989); **b** agpaitic index (AI) vs. SiO_2 diagram. The *dashed line* [AI = 0.87 (Liégeois and Black 1987)] separates alkaline and calc-alkaline granite series. Data are from previous studies (38 samples: Otlu and Boztug 1998; Boztug 1998, 2000) and present study (11 samples: listed in Table 3)

CS with high $(La/Yb)_N$ ratios reflect strong fractionation. REE abundances of CS (especially MREE and HREE) decrease as SiO_2 content increases and reflect strong fractional crystallization within CS itself. BR and CS define different trends in numerous trace-element diagrams (cf. Fig. 6). The contrasting slopes defined by samples from the two granite types in a Ba vs. Rb, $(La/Yb)_N$ vs. $(Eu/Eu^*)_N$, and $(Tb/Yb)_N$ vs. $(Eu/Eu^*)_N$ diagrams (Fig. 6) demonstrate, along with the chemical data shown in Figs. 3, 4 and 5 and the mineralogical data, that the BR and CS granitoids were not produced by fractional crystallization from a single magma source.

Although both rock suites display arc affinity based on their negative Nb, Ta, and Ti anomalies and Th enrichment relative to La, discrimination diagrams for the tectonic setting do not indicate arc setting. For instance, in the Rb vs. (Nb + Y) diagram (Fig. 7) of Pearce et al. (1984), CS rocks mostly plot in the within-plate granite (WPG) field, whereas the BR samples typically are scattered in the WPG and volcanic arc granite (VAG) fields, near to the junction of the VAG, WPG, and syn-collision (syn-COLG) fields. Such a contrast between the setting observed in the field and the setting inferred from trace-element discrimination diagrams is known from many collision settings, where late- and post-collisional magmatism shows the geochemical signature of the underlying collided crust rather than the tectonic setting of the last magmatism (e.g., Förster et al. 1997; Romer et al. 2001).

The BR samples are characterized by high Sr concentrations, negligible Eu anomalies, and depletion of HREE and Y relative to LREE. These features are indicative for a residue with garnet and amphibole, but without plagioclase. The concentration of incompatible elements (e.g., Ba = 773–1425 ppm, Th = 10–63 ppm, Nb = 15–37 ppm; data from Table 3 and Otlu and Boztug 1998; Boztug 1998, 2000) is much higher than for average continental crust (ACC; Ba = 390 ppm, Th = 5.6 ppm, Nb = 12 ppm, values from Rudnick and Fountain 1995). The BR rocks are typically characterized by higher Ba/Nb (34–87), Ba/Zr (2.4–6.3), La/Nb (2.7–3.4), Ce/Pb (17–31), Rb/Nb (5.4–12), K/Nb (1,600–3,000), Th/La (0.34–0.56), Th/Nb (0.43–3.3), Th/Yb (9.3–15), and Ta/Yb (0.59–0.61), and lower Ba/La (15–19) ratios than ACC. The observed enrichment in LILE and LREE relative to HFSE, and enrichment in HFSE relative to ACC may indicate either (1) contamination by continental crustal material during the ascent of the magma (e.g., DePaolo 1981) or (2) subcontinental lithospheric mantle (SCLM) source that is enriched by contribution of slab-derived components from an earlier subduction (e.g., Whalen et al. 1996). Both scenarios may yield identical chemical signatures and cannot be distinguished without isotope data. A derivation of these magmas from an enriched SCLM possibly provides the most straightforward explanation for the observed geochemical signatures, which are similar to subduction zone related magmas (e.g., Ba/Nb > 30, Gill 1981; high La/Nb, Hawkesworth et al. 1995; high Ba/Zr Ajaji et al. 1998; average Th: 18(±7) ppm, average Nb: 11(±4) ppm, Whalen et al. 1987). Ilbeyli et al. (2004) presented isotope data from the Baranadag granitoid that is characterized by a high initial $^{87}Sr/^{86}Sr$ (0.70804) and a low initial $^{143}Nd/^{144}Nd$ (0.51227) value. Ilbeyli et al. (2004) suggested a derivation of the Baranadag magmas from an enriched SCLM source and subsequent modification by crustal contamination in combination with fractional crystallization.

These geochemical features are reported not only from arc environments but also from enriched sources related to post-collisional environments (Whalen et al. 1996; Wenzel et al. 1997; Ajaji et al. 1998). Ajaji et al. (1998) suggests that such an enrichment in post-collisional setting was related to an earlier subduction event creating a subduction-modified SCLM source. Since

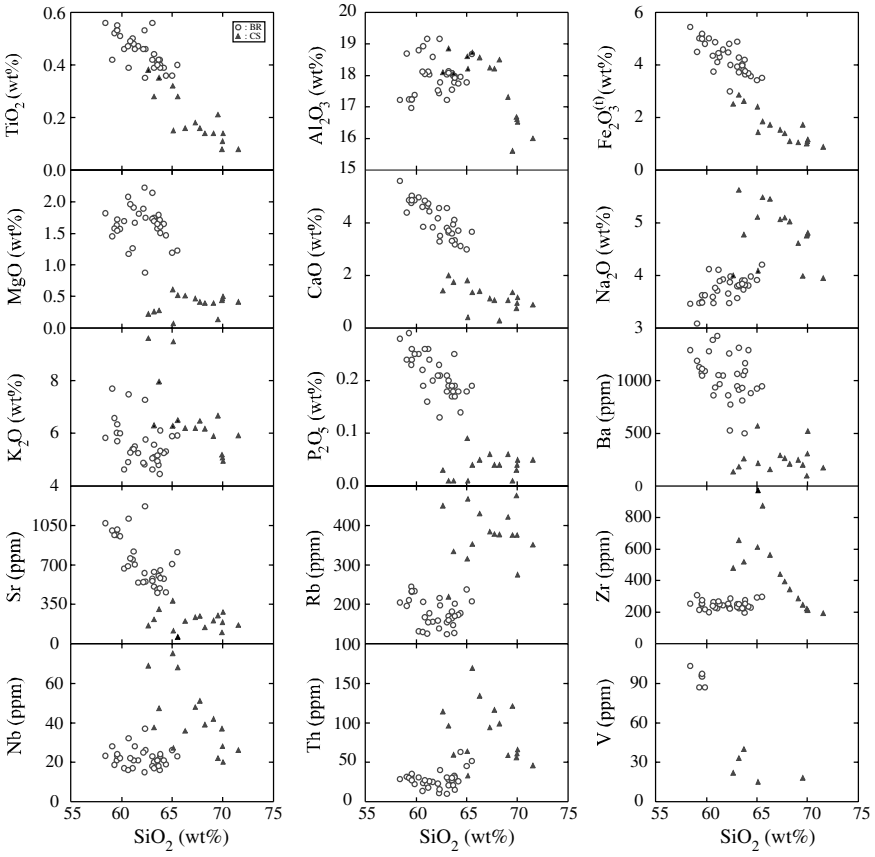

Fig. 3 Harker variation diagrams for selected major and trace elements of the BR and CS samples. Data sources as for Fig. 2

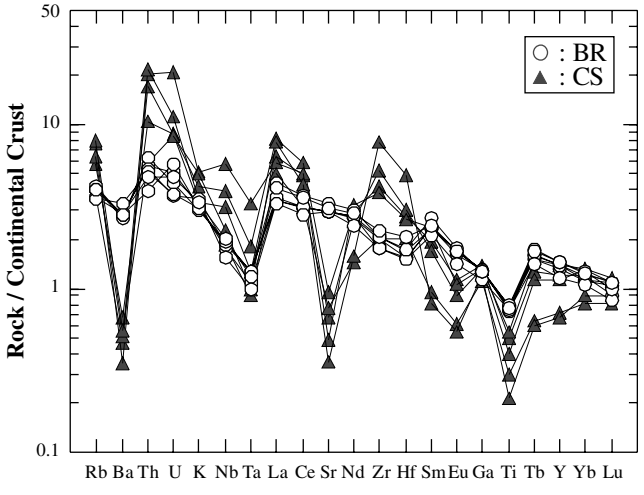

Fig. 4 Continental-crust-normalized (after Rudnick and Fountain 1995) multi-element variation diagrams of BR and CS. Data sources: Table 3

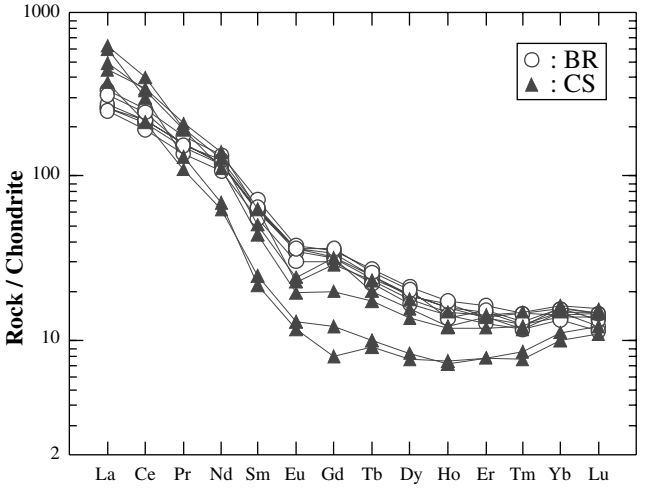

Fig. 5 Chondrite-normalized (after McDonough and Sun 1995) rare earth element pattern for the BR and CS granitoids. Data sources: Table 3

field and geochemical data suggest a post-collisional setting, the observed high LILE/HFSE and LREE/HREE ratios of the BR rocks are likely to reflect a source signature rather than the tectonic setting.

Even though the CS samples have variable Nb anomalies or even none and have also strong negative Ta and Ti anomalies, they display lower incompatible element ratios Ba/Nb (1.97–11.0), Ba/La (1.28–2.21), Ba/Zr (0.22–1.42), and Ce/Pb (8.50–10.6), but higher La/Nb (1.54–5.22) than the BR samples. These lower values reflect the strong depletion of Ba in the CS rocks, even lower than ACC, and the strong enrichment of Nb relative to ACC. The high LILE concentrations and the

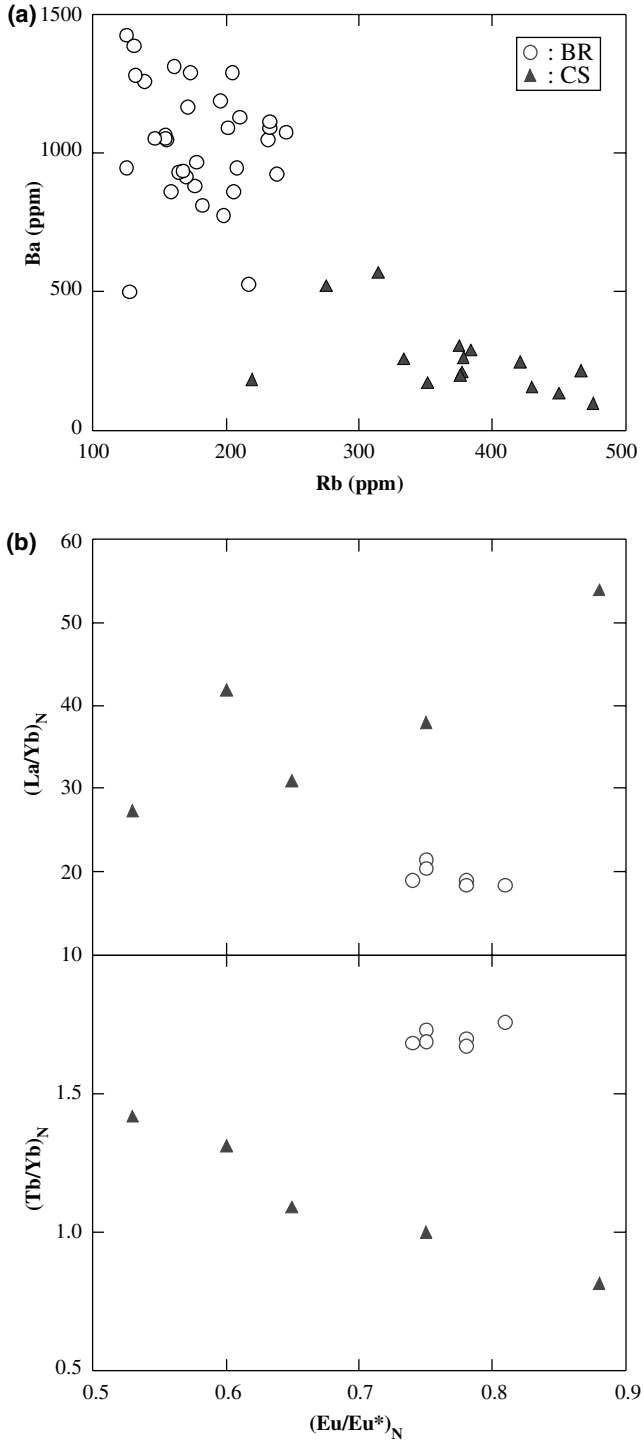

Fig. 6 **a** Ba vs. Rb; **b** $(La/Yb)_N$ vs. $(Eu/Eu^*)_N$; and **c** $(Tb/Yb)_N$ vs. $(Eu/Eu^*)_N$ diagrams for the BR and CS granitoids. Data sources: Table 3

enrichment of HFSE of the CS samples relative ACC may reflect an enrichment in the mantle source through ancient subducted material. Moreover, the enrichment in LILE such as Rb, K, and Ce, and high ratios of K/Nb, Rb/Nb, and Th/Nb suggest crustal contamination for CS.

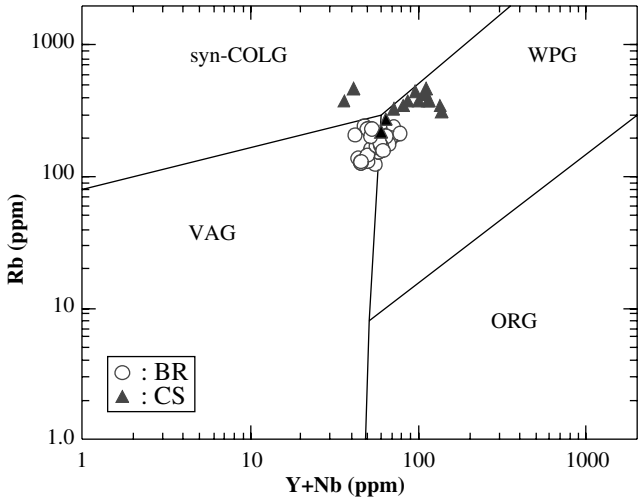

Fig. 7 Tectonic discrimination diagram (Rb vs. Y + Nb; Pearce et al. 1984) for the BR and CS granitoids (*VAG* volcanic arc granite, *syn-COLG* syn-collision granite, *ORG* ocean ridge granite, *WPG* within-plate granite). Data sources as for Fig. 2

Geochemical data indicate that the BR and CS granitoids have mantle sources, which have been modified by subduction-related components and experienced minor or no wall rock assimilation. Both of the granitoid suites do not represent the product of fractional crystallization from a single source and they are not genetically related to each other. Instead, they seem to have been generated in a post-collisional setting with WPG affinity. They are products from different sources, i.e., BR may be derived from a hybridized source and shows evidence of magma mingling/mixing and crustal contamination processes and CS reflects features common of A-type granitoids with significant crustal contamination.

Geochronology

Titanite forms abundant idiomorph crystals in both the BR and CS samples. Inclusion-free and fracture-free titanite was separated for U–Pb dating. For the correction of common Pb, K-feldspar was separated from the same specimens and leached before analysis (Romer et al. 1996).

Titanite from Baranadag has U contents ranging from 150 to 170 ppm and Pb_{tot} from 6.0 to 7.4 ppm (Table 4). Due to the rather high contents of common Pb (2.2–3.1 ppm), the measured $^{206}Pb/^{204}Pb$ is not very radiogenic (Table 4). In a $^{206}Pb/^{204}Pb$ – $^{238}U/^{204}Pb$ diagram, the data fall on a straight line that defines a considerably more radiogenic intercept than inferred from feldspar Pb. Using feldspar Pb to constrain the isochron results in excess scatter (MSWD = 2.7) and an age of 74.0 ± 2.8 Ma (2σ; Fig. 8a). The excess scatter originates dominantly from the feldspar Pb. There is a slight correlation between measured $^{206}Pb/^{204}Pb$ and $^{206}Pb/^{238}U$ age (Table 4) indicating that the use of a different common Pb correction could reduce the range

Table 4 U–Pb analytical data of titanite from granitoids of the Kaman Region, central Anatolia, Turkey

Sample[a]	Weight (mg)	Concentrations (ppm)		$^{206}Pb/^{204}Pb$	Radiogenic Pb (at %)[c]			Atomic ratios[c]				Apparent ages (Ma)[d]		
		U	Pb_{tot}	Measured ratios[b]	$^{206}Pb/^{204}Pb$	$^{207}Pb/^{204}Pb$	$^{208}Pb/^{204}Pb$	$^{238}U/^{204}Pb$	$^{206}Pb/^{238}U$	$^{207}Pb/^{235}Pb$	$^{207}Pb/^{206}Pb$	$^{206}Pb/^{238}U$	$^{207}Pb/^{235}U$	$^{207}Pb/^{206}Pb$
BR														
1	0.099	166	6.29	70.05	70.99	18.31	112.4	4,610	0.01144	0.08082	0.05123	73.3	79	250
2	0.122	159	6.55	67.56	68.25	18.10	115.2	4,260	0.01162	0.07809	0.04876	74.4	76	136
3	0.410	157	6.20	67.10	69.22	18.16	113.4	4,410	0.01143	0.07701	0.04885	73.3	75	141
4	0.187	148	6.04	67.59	68.07	18.16	111.6	4,220	0.01168	0.08078	0.05015	74.9	79	202
5	0.194	167	7.38	59.70	59.97	17.77	99.3	3,490	0.01182	0.08204	0.05035	75.7	80	211
6	0.245	158	6.76	62.14	62.40	17.88	102.3	3,700	0.01178	0.08163	0.05026	75.5	80	207
CS														
7	0.076	177	9.97	41.03	41.14	16.83	69.3	1,960	0.01138	0.07989	0.05090	73.0	78	236
8	0.120	185	9.22	47.22	47.37	17.05	78.6	2,500	0.01144	0.07503	0.04755	73.3	74	77
9	0.190	161	7.11	56.83	57.06	17.60	92.9	3,300	0.01160	0.07958	0.04975	74.4	78	183
10	0.252	157	8.46	44.50	44.57	17.04	74.9	2,210	0.01166	0.08377	0.05209	74.8	82	289
11	0.191	167	7.77	52.86	53.03	17.47	86.4	2,930	0.01170	0.08362	0.05182	75.0	82	277

[a]Titanite concentrates were obtained using standard mineral separation procedures and purified through separation by hand under the binocular. Care was taken to use only fracture-free and inclusion-free clear grains with distinct crystal surfaces. ^{205}Pb–^{235}U mixed tracer was added before sample dissolution. All samples were dissolved with 52% HF overnight on the hot plate, dried, and transferred overnight into chloride-form using 6 N HCl. Separation of Pb and U followed the ion-exchange chromatography described by Tilton (1973) and Manhès et al. (1978). Pb and U were loaded on single Re-filaments using a silica-gel emitter and H_3PO_4 (Gerstenberger and Haase 1997) and measured at 1,200–1,260 and 1,350–1,400°C for lead and uranium, respectively, on a Finnigan MAT262 multicollector mass-spectrometer using Faraday collectors and ion counting

[b]Lead isotope ratios corrected for fractionation with 0.1% / a.m.u

[c]Lead corrected for fractionation, blank, tracer contribution, and initial lead ($^{206}Pb/^{204}Pb = 18.77 \pm 0.10$, $^{207}Pb/^{204}Pb = 15.69 \pm 0.03$, $^{208}Pb/^{204}Pb = 38.90 \pm 0.20$). These values base on the measurement of leached K-feldspar samples that show within uncertainties identical isotopic compositions. BR: $^{206}Pb/^{204}Pb = 18.772$, $^{207}Pb/^{204}Pb = 15.700$, $^{208}Pb/^{204}Pb = 38.917$; CS: $^{206}Pb/^{204}Pb = 18.777$, $^{207}Pb/^{204}Pb = 15.686$, $^{208}Pb/^{204}Pb = 38.880$ (2σ uncertainties smaller than 0.1%). During the measurement period, total blanks were less than 5 pg for lead and less than 1 pg for uranium

[d]Apparent ages were calculated using the constants of Jaffey et al. (1971) recommended by IUGS (Steiger and Jäger 1977)

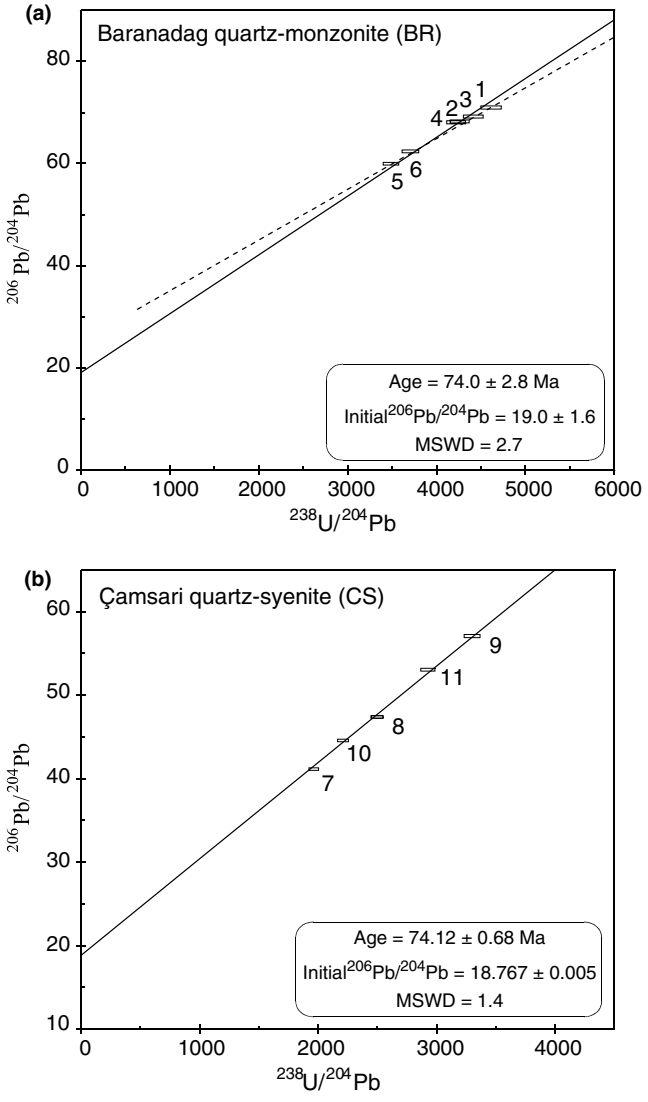

Fig. 8 $^{206}Pb/^{204}Pb$ vs. $^{238}U/^{204}Pb$ diagrams of **a** the BR; **b** the CS. The common Pb of feldspar is used to constrain the isochrons. The excess scatter for the data of the BR largely originates from the use of this common Pb that also influences to slope of the isochron (see text)

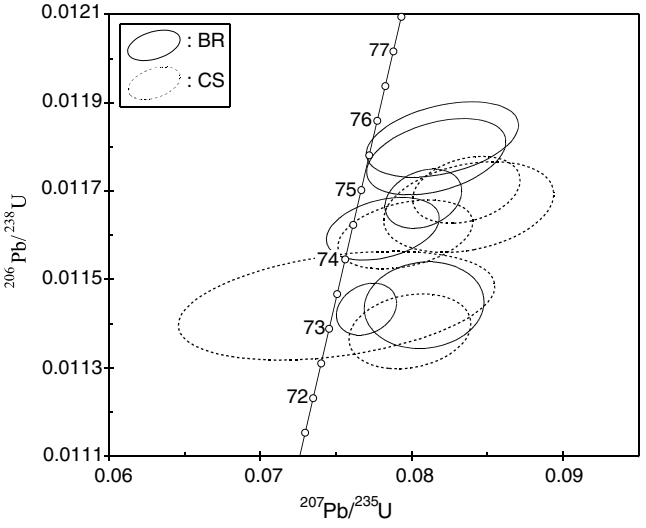

Fig. 9 $^{206}Pb/^{238}U$ vs. $^{207}Pb/^{235}U$ diagrams of the BR and the CS. Common Pb is corrected using the feldspar Pb from the dated samples. Although the data sets for both intrusions largely overlap, the range along the concordia is slightly larger for the BR samples, eventually resulting in a large age uncertainty

observed in $^{206}Pb/^{238}U$ ages. For a slightly more radiogenic common Pb, the scatter of the data would be reduced and the $^{206}Pb/^{238}U$ ages of the individual sample would be lowered. The anomalous pattern of the U–Pb data of Baranadag titanite may be explained by (a) a distinctly more radiogenic initial Pb, (b) heterogeneous initial Pb, and (c) partial disturbance of the U–Pb system of titanite during a later overprint. The BR experienced extensive magma mingling and assimilation. Therefore, the initial Pb isotopic composition of leached feldspar, which formed from a wide range of differently evolved melts, does not necessarily have to be homogeneous or to be representative for the dated titanite. (a) A more radiogenic initial Pb would reduce the age of the titanite samples considerably and require that titanite crystallized from a melt with a distinctly different Pb isotopic composition than recorded by feldspar, which is the major Pb carrier. A difference in initial Pb as indicated by the dashed regression through the titanite samples (Fig. 8a) is extremely unlikely. (b) Due to the non-radiogenic nature of the Pb in titanite, already a minor heterogeneity in the initial Pb of titanite becomes apparent as a range in $^{206}Pb/^{238}U$. For instance, a heterogeneity in the isotopic composition of initial Pb of only 0.5 U in $^{206}Pb/^{204}Pb$ results in an $^{206}Pb/^{238}U$ age range of 0.7 Ma. (c) A later recrystallization of titanite may have resulted in a loss of Pb, which would reduce the U–Pb age, or the incorporation of Pb, whose effect on the age depends on the isotopic composition of the Pb. Although the present data do not allow excluding any of these possible explanations, the freshness of the dated samples and their derivation from mixed sources may favor explanation (b). Such an explanation also may account for the way the data straddle along the concordia in the concordia diagram (Fig. 9). The use of a slightly higher $^{207}Pb/^{204}Pb$ for the correction of the initial Pb would have shifted the data to the left onto the concordia (Fig. 9).

Titanite from Çamsari has a similar range of U content (155–185 ppm; Table 4) as titanite from Baranadag. Due to its higher contents of initial common Pb (3.7–5.8 ppm), the Çamsari titanite has even lower $^{206}Pb/^{204}Pb$ (41.0 to 56.8, Table 3). In a $^{206}Pb/^{204}Pb$–$^{238}U/^{204}Pb$ diagram, the data fall on a straight line that intercepts the $^{206}Pb/^{204}Pb$ axis within uncertainties at the composition of feldspar Pb (Table 4). Using the feldspar Pb to additionally constrain the isochron yields an age of 74.1 ± 0.7 Ma (2σ; MSWD = 1.4; Fig. 8b). Similar to the titanite data from BR, titanite from CS shows some excess scatter in the concordia diagram and

plots slightly below the concordia. The scatter, however, is less pronounced (Fig. 9).

The titanite data shown in the concordia diagram have been calculated using the isotopic composition of leached feldspar for the common Pb correction. The data from both intrusions overlap entirely (Table 4). Using a more radiogenic Pb for the common Pb correction of the Baranadag intrusion would affect those samples most that show the oldest apparent $^{206}Pb/^{238}U$ ages, as these samples have the lowest $^{206}Pb/^{204}Pb$ (Table 4). Such a more radiogenic initial Pb would reduce the $^{206}Pb/^{238}U$ age of the Çamsari intrusion more than that of the Baranadag intrusion. The age overlap, however, persists as long no extreme values for the initial Pb are taken. The presented U–Pb titanite data, therefore, demonstrate that (1) there is no systematic difference in age between the two intrusions and (2) the ages are robust estimates for the time of emplacement of these granitoids.

Discussion and conclusions

Baranadag quartz-monzonite is identical to other H-type calc-alkaline granitoids in central Anatolia such as Yozgat, Agaçören, Ekecikdag, Behrekdag and Cefalikdag plutons, but it displays a transition to alkaline chemistry, which suggests a mature stage of post-collisional history (Aydin and Önen 1999). The U–Pb titanite age of 74.0 ± 2.8 Ma for BR agrees well with the paleontological constraints for the H-type granitoid at Terlemez, which is younger than Middle Turonian–Early Santonian (Yaliniz et al. 1997, 1999), i.e., 92–86 Ma according to the numeric time scale of Menning and Deutsche Stratigraphische Kommission (2002). The CS rocks are geochemically similar to other silica saturated A-type granitoids (e.g., Idisdagi and Hamit intrusions) throughout the CACC. The U–Pb titanite age of CS suggests that post-orogenic magmatism leading to the formation of silica-saturated A-type plutonic rocks in the CACC had started no later than 74.1 ± 0.7 Ma. The U–Pb titanite age of CS (74.1 ± 0.7 Ma) is identical to that of BR (74.0 ± 2.8 Ma) suggesting that the post-collisional H-type and A-type magmatism in the Kaman region are closely related in space and time and may have coevally tapped different sources in a very small area.

Subcontinental lithosphere may provide a potential source for syn- or post-collisional granitoid magmatism (Ben Othman et al. 1989). This subcontinental lithosphere may have high LILE/HFSE ratios due to earlier enrichment from dehydration and melting of sediments and/or basaltic crust of the subducted slab (e.g., Gill 1981). Such a modified SCLM could represent a likely source for the BR and CS granitoids. Melting of SCLM may have been caused by convective thinning of the lithosphere and/or delamination after collision and thickening (Turner et al. 1992; Platt and England 1994; Förster et al. 1997). According to these authors, hot upwelling asthenosphere rapidly replaces the lithosphere and eventually causes extension in the crust and melting of fluid-rich metasomatized parts of the lithospheric mantle (Platt and England 1994), producing highly incompatible element enriched melts (Turner et al. 1996; Hawkesworth et al. 1995). This kind of magmatism takes place pre-extensional or at the very onset of extension (Platt and England 1994; Hawkesworth et al. 1995). Turner et al. (1992) suggested that these magmatic episodes may play a role in transferring lithospheric mantle material and its compositional signature into the crust.

The post-collisional magmatism either dies out with minor amounts of evolved high-K calc-alkaline plutons or is replaced by alkaline magmatism (Liégeois et al. 1998). The BR and CS granitoids within the CACC are examples of such high-K calc-alkaline and alkaline magmatism, respectively, during the end of the post-collisional system. Thus, the U–Pb age data of BR and CS presented in this study suggest the post-collisional period of the Alpine orogeny may have ended around 74 Ma (Campanian, Menning and Deutsche Stratigraphische Kommission 2002) in central Anatolia.

Ilbeyli et al. (2004) stated that there is no localized extension in the CACC to generate the primary magmas for the granitoids. However, post-collisional extension giving way to the evolution of granitoids like BR and CS persisted in central Anatolia and resulted in the formation of extensional basins (e.g., Kizilirmak, Ulukisla, and Sivas basins) during the Late Maastrichtian to Paleocene (e.g., Dirik et al. 1999); 67–55 Ma according to the numerical time scale of Menning and Deutsche Stratigraphische Kommission (2002). Maastrichtian sediments at the basin margin are characterized by mass flows. The basin fill reaches up to 5,000 m thickness. Olistoliths of volcanic rocks in these basins are chemically related to shallow intrusions that represent equivalents of the deeper level A-type granitoids (Göncüoglu et al. 1997; Köksal et al. 2001). They have an alkaline character with geochemical affinities of within-plate type magmatism. Lower Tertiary volcanic rocks in these basins typically are represented by alkali basalts, trachytes, and trachyandesites (Gökten and Floyd 1987; Çevikbas and Öztunali 1992).

Even though reliable geochronological data are still lacking for many late- to post-collisional granitic intrusions of central Anatolia, our U–Pb data suggest that granitic magmatism related to the Alpine orogeny stopped in the Late Cretaceous. The new U–Pb data in conjunction with the regional occurrence of geochemically similar rocks are not compatible with geodynamic scenarios based on "granite intrusions of Paleocene-Early Eocene (e.g., Boztug 1998)" or "Paleocene-Early Eocene arc-type granitic plutonism" (e.g., Görür et al. 1984, 1998; Tüysüz et al. 1994; Erdogan et al. 1996).

Acknowledgements S. Köksal gratefully acknowledges access to laboratory facilities at the GeoForschungsZentrum Potsdam. We would like to thank S. Jung, K. Hammerschmidt and an anonymous reviewer for helpful and constructive reviews of this paper. We acknowledge the Scientific and Technical Research Council of Turkey (TUBITAK; project code YDABÇAG-101Y051) for supporting the geochemical analyses. S. Köksal also thanks K. Toksoy for help during the fieldwork.

References

Ajaji T, Weis D, Giret A, Bouabdellah M (1998) Coeval potassic and sodic calc-alkaline series in the post-collisional Hercynian Tanncherfi intrusive complex, northeastern Morocco: geochemical, isotopic and geochronological evidence. Lithos 45:371–393

Akiman O, Erler A, Göncüoglu MC, Güleç N, Geven A, Türeli K, Kadioglu YK (1993) Geochemical characteristics of granitoids along the western margin of the Central Anatolian Crystalline Complex and their tectonic implications. Geol J 28:371–382

Ataman G (1972) The preliminary study on the radiometric age of Cefalik Dagi that is one of the granitic-granidioritic bodies in the SW of Ankara (in Turkish). J Hacettepe Nat Appl Sci 2:44–49

Ayan M (1963) Contribution à l'étude pètrographique et géologique de la région située au Nord—Est de Kaman, vol 115. Publ Mineral Res Explor Inst Turkey, Ankara, pp 1–332

Aydin NS, Önen P (1999) Field, petrographic and geochemical features of the Baranadag quartz monzonite of the central Anatolian granitoids, Turkey. Turk J Earth Sci 8:113–123

Aydin NS, Göncüoglu MC, Erler A (1998) Latest Cretaceous magmatism in the Central Anatolian Crystalline Complex: review of field, petrographic and geochemical features. Turk J Earth Sci 7:259–268

Barbarin B (1990) Granitoids: mineral petrogenetic classifications in relation to origin and tectonic setting. Geol J 25:227–238

Bayhan H (1987) Petrographic and chemical-mineralogical characteristics of the Cefalikdag and Baranadag plutons (Kaman) (in Turkish). Geol Eng 30(31):11–16

Ben Othman D, White WM, Patchett J (1989) The geochemistry of marine sediments, island arc magma genesis, and crust-mantle recycling. Earth Planet Sci Lett 94:1–21

Bonin B, Azzouni-Sekkal A, Bussy F, Ferrag S (1998) Alkali-calcic and alkaline post-orogenic (PO) granite magmatism: petrological constraints and geodynamic settings. Lithos 45:45–70

Boztug D (1998) Post-collisional central Anatolian alkaline plutonism, Turkey. Turk J Earth Sci 7:145–165

Boztug D (2000) S-I-A-type intrusive associations: geodynamic significance of synchronism between metamorphism and magmatism in central Anatolia, Turkey. In: Bozkurt E, Winchester JA, Piper JDA (eds) Tectonics and magmatism in Turkey and the surrounding area. Geol Soc Spec Publ Lond 173:441–458

Çevikbas A, Öztunali Ö (1992) Geology of the Ulukisla-Çamardi (Nigde) Basin. Bull Miner Res Explor Inst Turkey 114:155–172

Collins WJ, Beams SD, White AJR, Chappell BW (1982) Nature and origin of A-type granites with particular reference to southeastern Australia. Contrib Mineral Petrol 80:189–200

Creaser RA, Price RC, Wormald RJ (1991) A-type granites revisited: assessment of a residual-source model. Geology 19:63–166

DePaolo DJ (1981) Trace element and isotopic effects of combined wall rock assimilation and fractional crystallization. Earth Planet Sci Lett 53:189–202

Didier J, Barbarin B (1991) Enclaves and granite petrology. Elsevier, Amsterdam, pp 1–625

Dirik K, Göncüoglu MC, Kozlu H (1999) Stratigraphy and pre-Miocene tectonic evolution of the southwestern part of the Sivas Basin, central Anatolia, Turkey. Geol J 34:303–319

Droop GTR (1987) A general equation for estimating Fe^{3+} concentrations in ferromagnesian silicates and oxides from microprobe analyses, using stoichiometric criteria. Miner Mag 51:431–435

Düzgören-Aydin NS, Malpas J, Göncüoglu MC, Erler A (2001) A review of the nature of magmatism in central Anatolia during the Mesozoic post-collisional period. Int Geol Rev 43:695–710

Eby GN (1990) The A-type granitoids: a review of their occurrence and chemical characteristics and speculations on their petrogenesis. Lithos 26:115–134

Eby GN (1992) Chemical subdivision of the A-type granitoids: petrogenetic and tectonic implications. Geology 20:641–644

Erdogan B, Akay E, Ugur MS (1996) Geology of the Yozgat region and evolution of the collisional Çankiri Basin. Int Geol Rev 38:788–806

Erkan Y, Ataman G (1981) An investigation on metamorphism age of central Anatolian massif by K–Ar method (in Turkish). J Hacettepe Univ Earth Sci 8:27–31

Erler A, Göncüoglu MC (1996) Geologic and tectonic setting of the Yozgat Batholith, northern central Anatolian crystalline complex, Turkey. Int Geol Rev 38:714–726

Erler A, Akiman O, Unan C, Dalkiliç F, Dalkiliç B, Geven A, Önen P (1991) The petrology and geochemistry of the Kirsehir massif magmatic rocks in Kaman (Kirsehir) and Yozgat regions (in Turkish). Turk J Eng Environ Sci 15:76–100

Förster HJ, Tischendorf G, Trumbull RB (1997) An evaluation of the Rb vs. (Y + Nb) discrimination diagram to infer tectonic setting of silicic igneous rocks. Lithos 40:261–293

Gerstenberger H, Haase G (1997) A highly effective emitter substance for mass spectrometric Pb isotope ratio determinations. Chem Geol 136:309–312

Gill JB (1981) Orogenic andesites and plate tectonics. Springer, Berlin Heidelberg New York, pp 1–385

Gökten E, Floyd PA (1987) Geochemistry and tectonic environment of the Sarkisla area volcanic rocks in central Anatolia, Turkey. Miner Mag 51:533–559

Göncüoglu MC (1986) Geochronological data from the southern part (Nigde Area) of the central Anatolian massif. Bull Miner Res Explor Inst Turkey 105–106:83–96

Göncüoglu MC, Türeli TK (1993) Petrology and geodynamic interpretation of plagiogranites from central Anatolian ophiolites (Aksaray-Turkey). Turk J Earth Sci 2:195–203

Göncüoglu MC, Türeli TK (1994) Alpine collision-type granitoids in the western central Anatolian crystalline complex. J Kocaeli Univ 1:39–46

Göncüoglu MC, Toprak GMV, Kusçu I, Erler A, Olgun E (1991) Geology of the western part of the central Anatolian massif: part I southern part (in Turkish). Unpublished Report 2909, Turk Petrol Co., Ankara

Göncüoglu MC, Erler A, Toprak V, Yaliniz K, Olgun E, Rojay B (1992) Geology of the western part of the central Anatolian massif: part II central part (in Turkish). Unpublished Report 3155, Turk Petrol Co., Ankara

Göncüoglu MC, Erler A, Toprak V, Olgun E, Yaliniz K, Kusçu I, Köksal S, Dirik K (1993) Geology of the central part of the central Anatolian massif: part III geological evolution of the Tertiary Basin of the central Kizilirmak (in Turkish). Unpublished Report 3313, Turk Petrol Co., Ankara

Göncüoglu MC, Köksal S, Floyd PA (1997) Post-collisional A-type magmatism in the central Anatolian crystalline complex: petrology of the Idis Dagi intrusives (Avanos, Turkey). Turk J Earth Sci 6(2):65–76

Görür N, Oktay FY, Seymen I, Sengör AMC (1984) Paleotectonic evolution of Tuzgölü basin complex, central Turkey: In: Dixon JE, Robertson AHF (eds) The geological evolution of the eastern Mediterranean. Geol Soc Spec Publ Lond 17:81–96

Görür N, Tüysüz O, Sengör AMC (1998) Tectonic evolution of the central Anatolian basins. Int Geol Rev 40:831–850

Güleç N (1994) Rb–Sr isotope data from the Agaçören Granitoid (East of Tuz Gölü): geochronological and genetical implications. Turk J Earth Sci 3:39–43

Güleç N, Kadioglu YK (1998) Relative involvement of mantle and crustal components in the Agaçören Granitoid (central Ana-

tolia-Turkey): estimates from trace element and Sr-isotope data. Chem Erde 58:23–37
Gündogdu NN, Bros R, Kuruç A, Bayhan H (1988) Rb–Sr whole-rock systematic of the Bayindir Feldspathoidal Syenites (Kaman-Kirsehir). In: Proceedings of the 20th Annual of Earth Science at Hacettepe University Symposium, Ankara, Abstract, p 55
Harris NBW, Pearce JA, Tindle AG (1986) Geochemical characteristics of collision-zone magmatism: In: Coward MP, Ries AC (eds) Collision Tectonics. Geol Soc Spec Publ Lond 19:67–81
Hawkesworth C, Turner S, Gallagher K, Hunter A, Bradshaw T, Rogers N (1995) Calc-alkaline magmatism, lithospheric thinning and extension in the Basin and Range. J Geophys Res 100:10271–10286
Ilbeyli N, Pearce JA (1997) Petrogenesis of the collision-related central Anatolian granitoids, Turkey. European Union Geosciences (EUG-9) Strasbourg, Abstract, p 502
Ilbeyli N, Pearce JA, Thirlwall MF, Mitchell JG (2004) Petrogenesis of collision-related plutonics in central Anatolia, Turkey. Lithos 72:163–182
Jaffey AH, Flynn KF, Glendenin LE, Bentley WC, Essling AM (1971) Precision measurements of half-lives and specific activities of ^{235}U and ^{238}U. Phys Rev Nucl Phys 4:1889–1906
Jung S, Mezger K, Hoernes S (1998) Petrology and geochemistry of syn- to post-collisional metaluminous A-type granites—a major and trace element and Nd–Sr–Pb–O-isotope study from the Proterozoic Damara Belt, Namibia. Lithos 45:147–175
Kadioglu YK, Güleç N (1999) Types and genesis of the enclaves in central Anatolian granitoids. Geol J 34:243–256
Kadioglu YK, Dilek Y, Güleç N, Foland KA (2003) Tectono-magmatic evolution of bimodal plutons in the central Anatolian crystalline complex, Turkey. Geol J 111:671–690
Köksal S, Göncüoglu MC, Floyd PA (2001) Extrusive members of postcollisional A-Type magmatism in central Anatolia: Karahidir volcanics, Idisdagi-Avanos area, Turkey. Int Geol Rev 43:683–694
Kuruç A (1990) Rb–Sr geochemistry of syenitoids from Kaman-Kirsehir region (in Turkish). Hacettepe University, Unpublished MSc Thesis, Ankara, pp 1–97
Kuscu I, Gençalioglu Kuscu G, Meinert LD, Floyd PA (2002) Tectonic setting and petrogenesis of the Çelebi granitoid, (Kirikkale-Turkey) and comparison with world skarn granitoids. J Geochem Expl 76:175–194
Liégeois JP, Black R (1987) Alkaline magmatism subsequent to collision in the Pan-African belt of the Adrar des Iforas. In: Fitton JG, Upton BGJ (eds) Alkaline igneous rocks. Geol Soc Spec Publ 30:381–401
Liégeois JP, Navez J, Hertogen J, Black R (1998) Contrasting origin of post-collisional high-K calc-alkaline and shoshonitic versus alkaline and peralkaline granitoids. The use of sliding normalization. Lithos 45:1–28
Lünel AT (1985) An approach to the naming, origin and age of Baranedag monzonite of Kirsehir intrusive suite. Middle East Tech Univ J Pure Appl Sci 18:385–404
Manhès G, Minster JF, Allegre CJ (1978) Comparative uranium–thorium–lead and rubidium–strontium study of the Saint Séverin amphoterite: consequences for early solar system chronology. Earth Planet Sci Lett 39:14–24
Maniar PD, Piccoli PM (1989) Tectonic discrimination of granitoids. Geol Soc Am Bull 101:635–643
McDonough WF, Sun S (1995) The composition of the Earth. Chem Geol 120:223–254
Menning M, Deutsche Stratigraphische Kommission (2002) Eine geologische Zeitskala 2002. Deutsche Stratigraphische Kommission (ed) Stratigraphische Tabelle von Deutschland 2002
Morimoto N (1988) Nomenclature of pyroxenes. Miner Petrol 39:55–76
Otlu N, Boztug D (1998) The coexistence of the silica oversaturated (ALKOS) and undersaturated (ALKUS) rocks in the Kortundag and Baranadag plutons from the central Anatolian alkaline plutonism, E Kaman/NW Kirsehir, Turkey. Turk J Earth Sci 7:241–257
Pearce JA, Harris NBW, Tindle AGW (1984) Trace element discrimination diagrams for the tectonic interpretation of granitic rocks. J Petrol 25:956–983
Platt JP, England PC (1994) Convective removal of lithosphere beneath mountain belts: thermal and mechanical consequences. Am J Sci 294:307–336
Romer RL (1994) Rb–Sr data structure—a possible cause for differences in Rb–Sr WR and U–Pb zircon ages. GFF 116:93–103
Romer RL, Schärer U, Steck A (1996) Alpine and pre-Alpine magmatism in the root-zone of the western central Alps. Contrib Mineral Petrol 123:138–158
Romer RL, Förster HJ, Breitkreuz C (2001) Intracontinental extensional magmatism with a subduction fingerprint: the late Carboniferous Halle Volcanic Complex (Germany). Contrib Mineral Petrol 141:201–221
Rudnick RL, Fountain DM (1995) Nature and composition of the continental crust: a lower crustal perspective. Rev Geophys 33:267–309
Sengör AMC, Yilmaz Y (1981) Tethyan evolution of Turkey: a plate tectonic approach. Tectonophysics 75:181–241
Seymen I (1981) Stratigraphy and metamorphism of the Kirsehir massif around Kaman (in Turkish). Geol Bull Turkey 24:101–108
Steiger RH, Jäger E (1977) Subcommission on geochronology: convention on the use of decay constants in geo- and cosmochronology. Earth Planet Sci Lett 36:359–362
Sylvester PJ (1989) Post-collisional alkaline granites. J Geol 97:261–280
Tatar S, Boztug D, Harlavan Y, Arehart GB (2003) The composite Behrekdag batholith: an igneous record for the collision between Anatolides and Pontides along Izmir–Ankara–Erzincan Zone around Kirikkale region, central Anatolia, Turkey. In: 56th geological congress of Turkey, Ankara, Abstract, pp 28–31
Tilton GR (1973) Isotopic lead ages of chondritic meteorites. Earth Planet Sci Lett 19:321–329
Toksoy-Köksal F, Göncüoglu MC, Yaliniz K (2001) Petrology of the Kurancali phlogopite metagabbro: an island arc-type ophiolitic sliver in the central Anatolian crystalline complex. Int Geol Rev 43:624–639
Turner SP, Sandford M, Foden J (1992) Some geodynamic and compositional constraints 'postorogenic' magmatism. Geology 20:931–934
Turner SP, Arnaud N, Liu J, Rogers N, Hawkesworth C, Harris N, Kelley S, van Calsteren P, Deng W (1996) Post-collision, shoshonitic volcanism on the Tibetian plateau: implications for convective thinning of the lithosphere and the source of ocean island basalt. J Petrol 37:45–71
Tüysüz O, Dellaloglu AA, Terzioglu N (1994) A magmatic belt within the Neo-Tethyan suture zone and its role in the tectonic evolution of northern Turkey. Tectonophysics 243:173–191
Wendt I (1993) Isochron or mixing line? Chem Geol 104:301–305
Wenzel T, Mertz DF, Oberhaensli R, Becker T, Renne PR (1997) Age, geodynamic setting, and mantle enrichment processes of a K-rich intrusion from the Meissen massif (northern Bohemian massif) and implications for related occurrences from the mid-European Hercynian. Geol Rundsch 86:556–570
Whalen JB, Currie KL, Chappell W (1987) A-type granites: geochemical characteristics, discrimination and petrogenesis. Contrib Mineral Petrol 95:407–419
Whalen JB, Jenner GA, Longstaffe FJ, Robert F, Gariéty C (1996) Geochemical and isotopic (O, Nd, Pb and Sr) constraints on A-type granite petrogenesis based on the Topsails igneous suite, Newfoundland Appalachians. J Petrol 37:1463–1489
Whitney DL, Dilek Y (1997) Core complex development in central Anatolia. Geology 25:1023–1026
Whitney DL, Teyssier C, Fayon AK, Hamilton MA, Heizler M (2003) Tectonic controls on metamorphism, partial melting, and intrusion: timing and duration of regional metamorphism

and magmatism in the Nigde Massif, Turkey. Tectonophysics 376(1–2):37–60

Wu F, Sun D, Huimin L, Jahn B, Wilde S (2002) A-type granites in northeastern China: age and geochemical constraints on their petrogenesis. Chem Geol 187:143–173

Yaliniz MK, Floyd PA, Göncüoglu MC (1996) Supra-subduction zone ophiolites of central Anatolia: geochemical evidence from the Sarikaraman ophiolite, Aksaray, Turkey. Miner Mag 60:697–710

Yaliniz MK, Parlak O, Özkan-Altiner S, Göncüoglu MC (1997) Formation and emplacement ages of supra-subduction-type ophiolites in central Anatolia: Sarikaraman ophiolites, central Turkey. In: 20th anniversary of geol education, Çukurova University, Adana, Abstract, pp 61–62

Yaliniz MK, Aydin NS, Göncüoglu MC, Parlak O (1999) Terlemez quartz monzonite of central Anatolia (Aksaray-Sarikaraman): age, petrogenesis and geotectonic implications for ophiolite emplacement. Geol J 34:233–242